First-principles study of the structural and electronic properties of bulk ZnS and small Zn_nS_n nanoclusters in the framework of the DFT + U method

Manas Sharma and Debabrata Mishra*
Department of Physics and Astrophysics, University of Delhi, New Delhi 110007, India

Jagadish Kumar
Department of Physics, Utkal University, Bhubaneswar 751004, India

(Received 22 May 2019; revised manuscript received 5 July 2019; published 31 July 2019)

We investigate the structural and electronic properties of bulk ZnS in zinc blende as well as in wurtzite phase, and Zn_nS_n nanoclusters by using the Hubbard model (DFT + U). It provides an on-site Coulomb correction to mitigate some of the commonly known limitations of traditional DFT-GGA method such as the underestimation of band gap and inaccurate description of electronic band structure. Especially for the nanoclusters, the traditional DFT method cannot reproduce all properties accurately that are observed in the experiments. Within the framework of DFT + U method, our model is first able to predict various properties of bulk ZnS (zinc blende and wurtzite) as well as in nanoclusters with high accuracy. We empirically determined the Hubbard correction parameters U_d and U_p for Zn-3d and S-3p states, respectively, that could reproduce the measured values of band gaps, d-band positions, p-states bandwidths, lattice parameters, etc. with a reasonable agreement. It was found that our model can be compared very well with more accurate hybrid functionals at only a fraction of the computational cost. Further, the selected pair of U_d and U_p values are used to investigate the structural and electronic properties of ZnS nanoclusters and results agree well with the higher levels of theory.

DOI: 10.1103/PhysRevB.100.045151

I. INTRODUCTION

II-VI semiconductors including ZnS, CdS nanoclusters have been a subject of immense interest for scientists due to their unique optoelectronic [1] properties emerging out of quantum confinement effect and find potential applications in next generation solar cells, light-emitting diodes, liquid crystal displays, and photodetectors [2–5]. In particular, ZnS offers peculiar optical properties such as a wide direct band gap (≈3.7–3.9 eV) [6,7] and transparency in an extremely wide energy range. It also exhibits polymorphism and is usually found in two phases such as hexagonal wurtzite (wz: P63mc) and cubic zinc-blende phase (zb: F$\bar{4}$3m). The zb phase is known to be more stable at low temperatures than the wz phase which is stable at high temperatures (1020° C). Synthesis of ZnS nanostructures in the form of nanoribbons, nanotubes, and nanowires have been successful and can be found in the literature [3–5]. Nevertheless, preparation of ZnS nanocluster is extremely difficult due to its metastable and agglomeration behavior. These nanoclusters also differ drastically from their bulk phases unlike quantum dots, where the bulk crystal structure is still somewhat preserved. On account of this, the definitive prediction and/or correlation of structure and optoelectronic properties of ZnS nanoclusters is perplexing. Therefore, it is crucial to carefully investigate the interplay of structural and electronic properties to understand and improve the performance of device both experimentally and theoretically.

Among the whole set of quantum mechanical (QM) tools available for this purpose, density functional theory (DFT) offers a reasonable level of accuracy at cheap computational cost and hence, is suitable for our study. Common DFT methods using local density approximation (LDA) [8] or generalized-gradient approximation (GGA) [9] to the exchange-correlation functional are known to describe the physical properties fairly but severely fail to describe the electronic properties of Zn chalcogenides, resulting in drastic underestimation of band gaps by 40–50% with respect to measured values [7,10]. Moreover, the energy of the occupied d manifold is overestimated by 3 eV and shows spurious hybridization of p-d levels [10,11]. Therefore, for a reliable theoretical study of ZnS nanoclusters it is important that we first remedy the aforementioned shortcomings. Such problems arise due to the following reasons: (i) lack of derivative discontinuity in the exchange-correlation energy in traditional functionals such as LDA or PBE-GGA [12–14] and (ii) the self interaction error that over-delocalizes the occupied states moving them upwards in energy range [8]. Several approaches have been proposed to rectify these problems, such as LDA plus self-interaction correction (LDA-SIC) [8], self-interaction-relaxation correction (SIRC-LDA) [15], GW approximation [16], DFT + U [17,18], and hybrid functionals [19,20].

The mean-field Hubbard correction, commonly known as DFT + U and introduced by Liechtenstein and Anisimov [17,18], has gained a lot of popularity due to it's cheap computational cost and accuracy in correction for the overdelocalization of the d electrons, especially in transition metals. DFT + U introduces an on-site Coulomb interaction U

*dmishra@physics.du.ac.in

(Hubbard parameter) that favors the localization of states. DFT + U is particularly needed for strongly correlated, i.e., $U/W > 1$, where W is the bandwidth and intermediately correlated ($U/W \sim 1$) systems [21]. Hubbard parameters can be computed using linear response approach as described by Cococcioni *et al.* [22], however, this method is not suitable for closed shell systems such as Zn where the localized bands are completely filled and insensitive to linear perturbations. Other *ab initio* methods are constrained LDA (cLDA) [23] and constrained random-phase approximation (cRPA) [24] which are computationally expensive. Considering the sufficient amount of experimental data already available for ZnS we chose to determine the Hubbard parameters by fitting the electronic band structure to the experimental values.

Matxain *et al.* [25] and many others [26–28] have studied the small ZnS nanoclusters using the B3LYP [29,30] hybrid exchange-correlation functional with local basis sets, which is known to give reliable results. B3LYP has been known to be significantly more expensive than the GGA functionals, especially with plane waves as the basis sets as compared to local (atom centered Gaussian) basis sets. But many materials simulation packages such as VASP and QUANTUM ESPRESSO [31] offer only plane-wave basis sets and therefore performing accurate calculations would require a lot of computational resources which aren't accessible to everyone. This poses an obstruction to the development of high-throughput quantum mechanics [32] which relies on the accurate prediction of the electronic properties of materials at cheap computational costs. We also compare the findings of other GGA (plane-wave) based studies [33]. Thus, the paper primarily consists of two parts. The first part deals with the determination of suitable Hubbard parameters by studying the influence of Hubbard correction term on the structural and electronic properties of bulk ZnS. In the second part we employ the selected Hubbard parameters to investigate the structural, electronic, and optical properties of ZnS nanoclusters of different sizes. This study hopes to help develop an accurate theoretical model to assist in the development of ZnS nanoclusters in supporting future technologies.

II. COMPUTATIONAL DETAILS

The plane-wave calculations were carried out by using the QUANTUM ESPRESSO [31] package. Different shapes of cluster structure are designed by using the software VESTA [34], BURAI [35], and JMOL [36]. The exchange-correlation functional (xc) is approximated using the generalized gradient approximation (GGA) in the parametrization of Perdew, Burke, and Ernzerhof (PBE) [9]. The interaction between the nuclei and the electrons is modelled using ultrasoft pseudopotentials (PPs) [37]. The 3d and 4s electrons of Zn, and 3s and 3p electrons of S, were treated as valence electrons in the PPs. The Kohn Sham orbitals and the charge density are represented using basis sets consisting of plane waves up to a maximal kinetic energy of 55 Ry and 440 Ry, respectively, for both zb and wz ZnS, which were determined by observing the convergence of the total energy with the increase in plane wave kinetic energy (variational principle). A $6 \times 6 \times 6$ Monkhorst-Pack (MP) [38] grid, which yields 10 k points in the irreducible Brillouin zone (IBZ), was determined to be sufficient for the zinc blende structure while an $8 \times 8 \times 6$ MP grid, with 196 k points in the irreducible Brillouin zone, was used for the wurtzite structure. For the initial configuration we used the experimental lattice parameters for both the phases [39,40]. Structural parameters were then optimized by quasi-Newton ionic relaxation using the Broyden, Fletcher, Goldfarb, Shanno (BFGS) algorithm [41–44]. The convergence criterion for the bulk optimization was 10^{-5} Ry for energy, 0.00025 eV/Å for force. The DFT + U calculations were performed using the simplified version of rotationally invariant scheme [22]. Influence of the Hubbard corrections, when applied to both Zn-3d and S-3p orbitals, was studied in the following manner. First, the Hubbard parameter, U_d, is added to only Zn-3d orbitals ranging from 2 eV to 14 eV in steps of 2 eV. Then, the Hubbard parameter, U_p, is applied to S-3p states along with U_d where the U_p values range from 1 eV to 9 eV. Initial geometries for nanoclusters were designed by consulting previous studies [25–28,33]. These were put inside a cubic unit cell with at least 15 Å of vacuum on all sides to get rid of any periodicity induced effects. These were then optimized using the BFGS algorithm and Hubbard corrections until the forces were reduced to less than 0.01 eV/Å per atom. We also performed a few nanocluster calculations using the newer definitions of TZVP (triple-ζ valence polarization) [45] basis set and B3LYP xc functional (to see whether the results corroborate with the plane-wave DFT + U results), for which we employed the ORCA package [46]. The convergence criterion for the geometry optimization for these calculations was 10^{-5} Ry for energy and 0.015 eV/Å for forces.

III. RESULTS AND DISCUSSION

A. Determination of appropriate Hubbard parameters (U_p and U_d) for bulk ZnS

1. Standard DFT

The wz phase has the space group P63mc with experimental lattice parameters: $a = b = 3.822$ Å and $c = 6.260$ Å [39]. The lattice parameter a of zb phase with space group F$\bar{4}$3m is measured to be 5.409 Å [40]. Our standard DFT-GGA calculations predict the lattice parameter a, of zb-ZnS at 5.447 Å which is greater than the experimental 5.409 Å. Similarly, for wz-ZnS, the calculated lattice parameters: $a = 3.849$ Å and $c = 6.309$ Å are marginally overestimated as compared to the experimental values.

The calculated GGA band gaps for wz-ZnS and zb-ZnS are 2.06 eV and 2.01 eV, respectively, which are severely underestimated by ≈45% as compared to the measured values: 3.7 eV for zb and 3.86 eV for wz-ZnS [6,7]. Figure 1(a) and Fig. 2(a) show the band structures and density of states for wz and zb phases, respectively, obtained using standard DFT. Due to tetrahedral symmetries of both the phases, the distribution of states is very similar for both the structures. The top of the valence band is composed of mainly S-3p states. The lowest energy manifolds (below −10 eV) are rather narrow and entirely of S-3s character. The cation (Zn) d-band and anion (S) p-band show slight hybridization. The spurious p-d states hybridization in ZnS is attributed to the

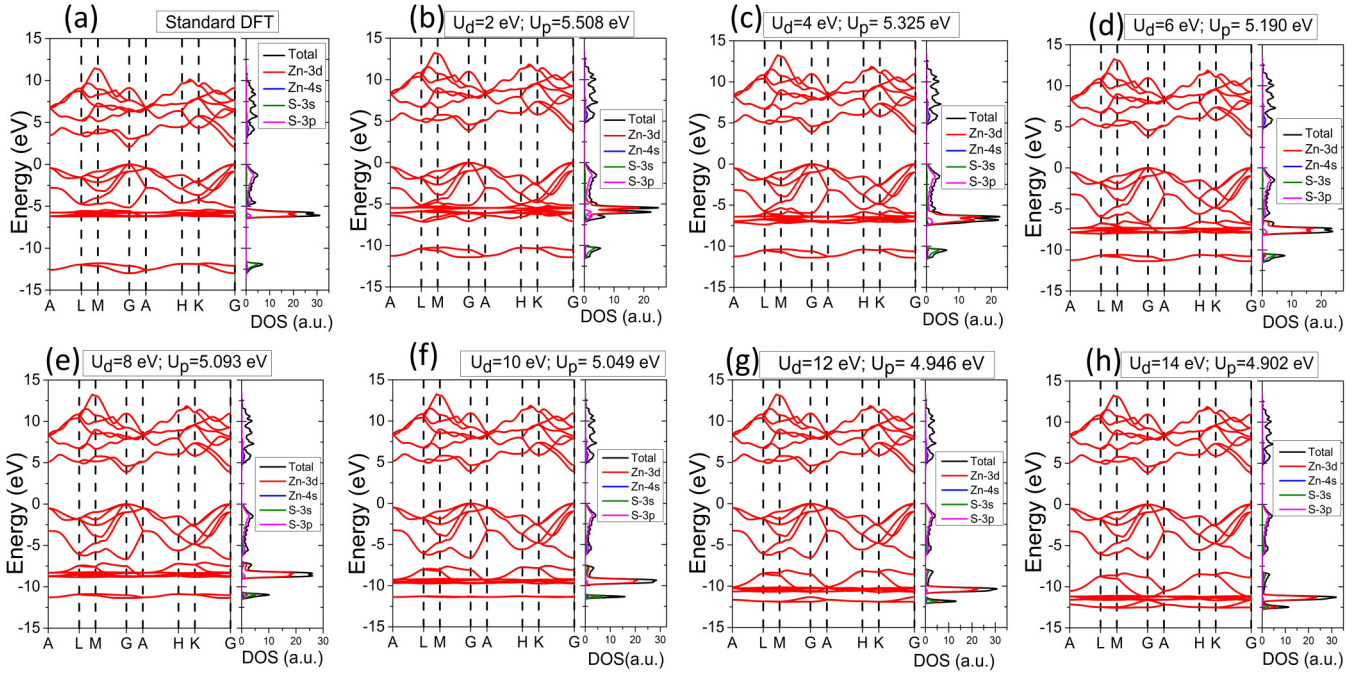

FIG. 1. Band structures and DOS for wz-ZnS using, (a) Standard DFT, (b-h) DFT + U with the selected values of U_p and U_d given in Table II.

inefficiency of the traditional DFT to account for the self interaction energy error, which results in overdelocalization of electrons. The valence band is dominated by the S-3p orbital states, while the conduction band is dominated by the Zn-4s orbital states. The average energy of d-band states at Gamma (G) point is −5.89 eV and −5.95 eV for zb and wz phases, respectively, which is very far from the experimental ∼− 9 eV [11,15,47]. The valence p bandwidth is ∼− 5.14 eV for both the phases which is in good agreement with the experimental value of −6.4 eV [11]. The values we got are similar to the other reported values in the literature using GGA as xc [10,15,32].

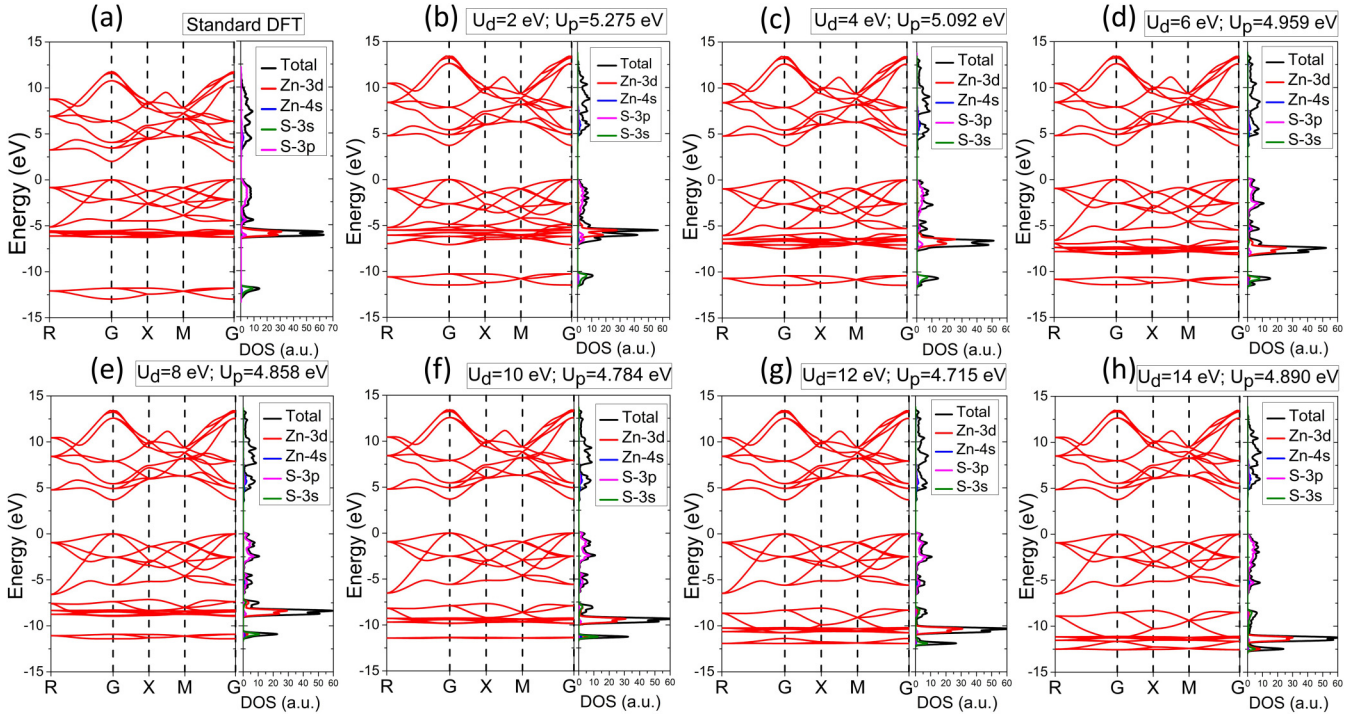

FIG. 2. Band structures and DOS for zb-ZnS using (a) standard DFT, (b)–(h) DFT + U with the selected values of U_p and U_d given in Table I.

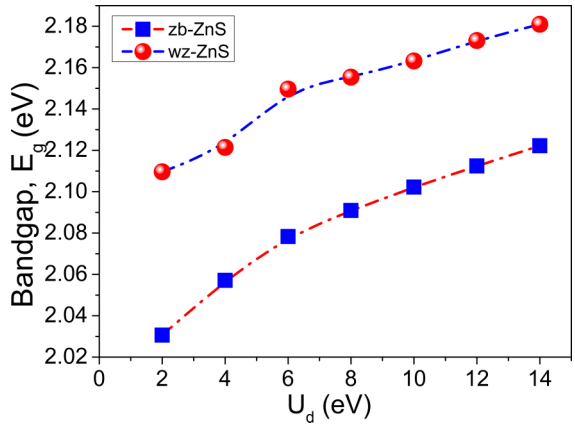

FIG. 3. Variation of band gap (E_g) with U_d ($U_p = 0$) for zb-ZnS and wz-ZnS. (The dash-dot lines are B-spline interpolation of the simulated data points and serve as a guide to the eye.)

2. *Effect of U_d*

The variation of band gap (E_g), with U_d ($U_p = 0$) for both wz-ZnS and zb-ZnS is shown in Fig. 3. In both the cases, E_g increases with U_d, but very insignificantly. Even at $U_d = 14$ eV, the band gap is still at least 1.6 eV less than the measured values. Figure 4 shows the variation of structural parameters with the application of U_d for both the phases. The lattice parameters for both zb-ZnS and wz-ZnS increase with increasing U_d, which is undesirable as GGA already overestimated the parameters. The c/a ratio, however, for the wz phase, remained almost constant at ∼1.639, as shown in Fig. 4, similar to what we got by GGA and in very good agreement with the experimental 1.638. Therefore, the application of U_d alone is nowhere enough to reproduce the measured band gap or the structural parameters. The band gaps are severely underestimated, while the lattice parameters are slightly overestimated.

3. *Effect of U_p*

In traditional formulation of DFT + U the correction term U has been based explicitly on the localization of the d orbitals and is not used for the p or s orbitals which tend to be less localized compared to d electrons. However, on analyzing the Löwdin charges [48] on S atoms we found that the electrons were slightly overdelocalized giving an ionicity of ∼0.5 which is a little less than the expected value of ∼0.7. Therefore, Hubbard correction could indeed help in localizing the S atom electrons sufficiently. Many other groups have reported similar findings for transition metal oxides and chalcogenides [32,49]. Figures 5 and 6 show the variation of band-gap and structural parameters with U_p (for a given U_d) for zb and wz phases, respectively. Both the lattice parameters and the band gaps show high sensitivity to the application of U_p along with U_d. In contrast to the increase of band-gap with increasing U_p, the lattice parameters are found to decrease monotonically with increasing U_p (for a given U_d) for both the phases. This is attributed to the strong localization of the valence electron states ($3p$) of S atoms. This leads to less repulsion between the atoms and hence a reduced lattice parameter with increasing U_p. The same phenomenon is also observed in wz-ZnO [50]. The effect of U_p on a is slightly more than c, as seen from the decreasing value of c/a ratio. Therefore, the decrease in volume is not isotropic. U_p enhances the band gap significantly and can even exceed the experimental values. Experimental values of lattice parameters and band gaps for both the phases are reached for similar values of $U_p \sim 5$ eV for all U_d. This shows that U_p plays a significant role in correct prediction of properties of ZnS. Further analysis is carried out by performing band structure and DOS calculations on a few select pair of Hubbard parameters (U_p and U_d) on the basis of their ability to reproduce the measured band gaps: 3.7 eV for zb-ZnS and 3.86 for wz-ZnS. This is done by performing linear fits to the band-gap curves in Fig. 5 and Fig. 6. Tables I and II show the seven selected pairs of U_d and U_p along with the analysis of electronic energies and structural parameters for zb and wz phase, respectively. Figure 1 and Fig. 2 show the band structures and DOS calculated for corresponding selected pairs of U_d and U_p for zb and wz-ZnS, respectively. The trends observed for band energies are similar for both the structures. It is observed that increasing U_d value shifts the Zn-$3d$ band downwards and reduces the p-d repulsion with the S-$3p$ band which in turn shifts the valence band maximum (VBM) downwards, thereby increasing the band gap. However, once the d states are completely disentangled from the p states, the band gap becomes insensitive to further increment in U_d. This is observed by small changes in E_g with increasing U_d as seen in Fig. 3. In addition to that, Table I and Table II illustrate that increasing U_d, when U_p values are almost the same, reduces the d-band energies but doesn't affect the band gaps much. The rigid shift of the bands arises

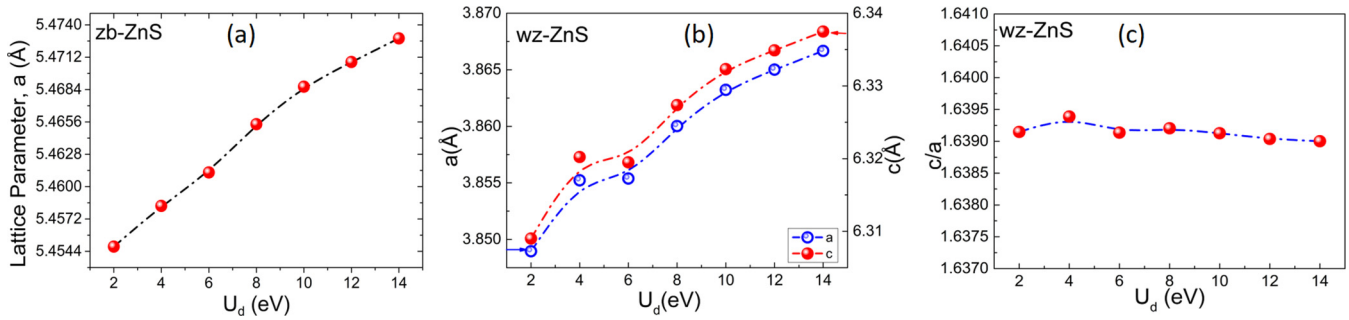

FIG. 4. Variation of structural parameters with U_d for (a) zb-ZnS and (b),(c) wz-ZnS. (The dash-dot lines are B-spline interpolation of the simulated data points and serve as a guide to the eye.)

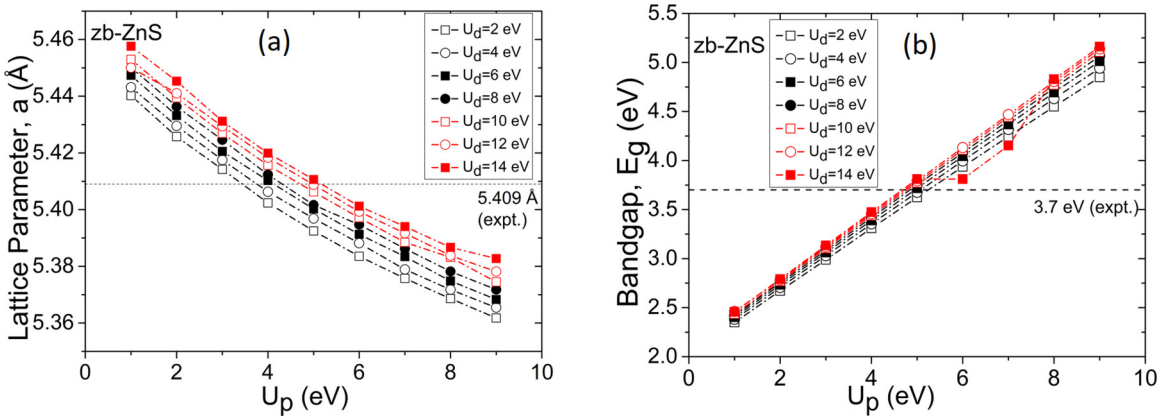

FIG. 5. Variation of lattice parameter (a) and band gap E_g (b) with U_p for different U_d for zb-ZnS.

from a singularity due to the filled character of the Zn-3d_{10} band and is elaborately discussed in Ref. [49]. The positions of VBM and CBM remained almost the same for all the pairs of U_p and U_d. As U_d was increased, a slightly smaller value of U_p was needed to achieve the experimental band gap. High U_d values of 8 and 10 eV give d-band positions in the range $-8.4 < E_d < -9.4$ for both wz and zb-ZnS, which are very close to the experimental value of -9 eV for both the phases. Other properties such as p-valence bandwidth and lattice parameters also seem to be in good reasonable agreement with the measured values for the selected pairs of U_p and U_d (especially those corresponding to $U_d = 10$ eV). One can therefore say that treating the band gaps and d-band energies as benchmarks, we are able to reproduce the experimental structural properties well.

The optimum choice for Hubbard parameters (U_p^{opt} and U_d^{opt}) is found by finding the pair of U_p and U_d corresponding to which the deviations from measured electronic and structural properties are the least. Using this criteria, we propose the optimum pair $U_d^{\text{opt}} = 10$ eV and $U_p^{\text{opt}} = 4.784$ eV for the

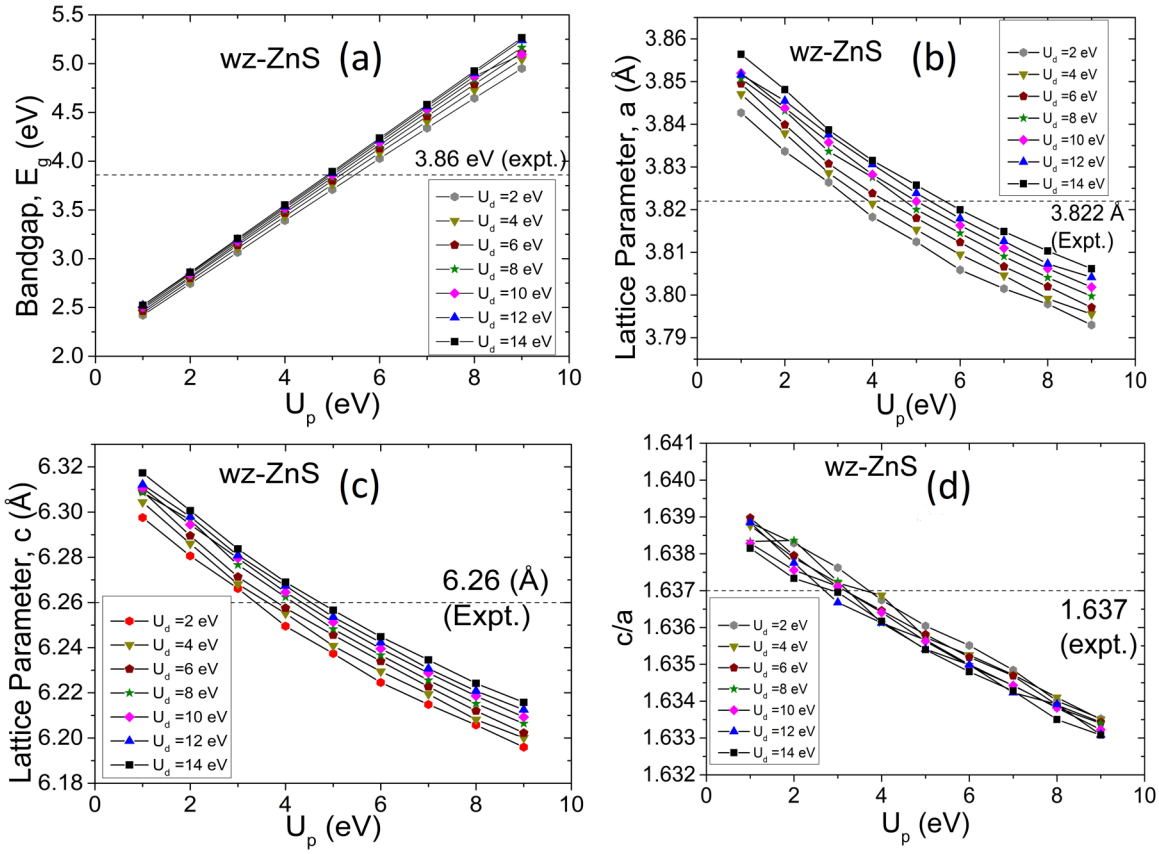

FIG. 6. (a) Variation of band gap (E_g) and (b)–(d) structural parameters with U_p for different U_d for wz-ZnS. The dashed lines correspond to the experimental values.

TABLE I. Calculated lattice parameters and electronic band properties for the selected pairs of U_p and U_d for the zinc blende phase obtained by fitting to the experimental band gap of 3.7 eV. a: lattice parameter; E_g: band gap; E_d: cation average d-band energy at the Gamma point; W_p: anion p valence bandwidth. Experimental values are from Refs. [6,11,15,40,47].

U_d(eV)	U_p(eV)	a (Å)	E_g(eV)	$E_d(G)$(eV)	W_p(eV)
2	5.275	5.389	3.710	−5.876	−5.22
4	5.092	5.395	3.707	−6.682	−6.03
6	4.959	5.399	3.706	−7.535	−6.60
8	4.858	5.404	3.702	−8.404	−6.58
10	4.784	5.408	3.701	−9.274	−6.53
12	4.715	5.411	3.697	−10.139	−6.46
14	4.89	5.411	3.773	−10.917	−6.50
Expt.		5.409	3.70	−9.0	−6.40

TABLE II. Calculated lattice parameters and electronic band properties for the selected pairs of U_p and U_d for the wurtzite phase obtained by fitting to the experimental band gap of 3.86 eV. a, c: lattice parameters; E_g: band gap; E_d: cation average d-band energy at the Gamma point; W_p: anion p valence bandwidth. Experimental values are from Refs. [7,11,15,39,47].

U_d (eV)	U_p (eV)	a (Å)	c(Å)	c/a	E_g (eV)	$E_d(G)$	W_p (eV)
2	5.508	3.808	6.230	1.635	3.871	−5.943	−5.15
4	5.325	3.812	6.235	1.635	3.870	−6.738	−5.96
6	5.190	3.816	6.242	1.635	3.864	−7.564	−6.62
8	5.093	3.819	6.246	1.635	3.863	−8.459	−6.67
10	5.049	3.821	6.250	1.635	3.873	−9.358	−6.63
12	4.946	3.823	6.254	1.635	3.859	−10.270	−6.56
14	4.902	3.826	6.257	1.635	3.859	−11.128	−6.52
Expt.		3.822	6.260	1.638	3.86	−9.0	−6.4

zb phase and $U_d^{\text{opt}} = 10$ eV and $U_p^{\text{opt}} = 5.049$ eV for the wz phase. Note that the U_p^{opt} values for both the phases are very similar, with the difference accounting for the larger band gap of the wz phase.

The optimum U_p^{opt} and U_d^{opt} values model the band structure and structural properties better than many approximations such as GW, HSE, etc. [16,32]. These values, although they appear to be high, are in keeping with what others have reported [32,49,50]. The rest of the DFT + U calculations in this paper are performed using the optimum values for both the phases. We also perform further analysis to see the ability of our proposed values in predicting the effective masses of charge carriers, bulk modulus, and DOS features.

4. Density of states

ZnS has novel potential applications in various fields because of its structure dependent properties. In order to understand the electronic properties we have calculated the total density of states (TDOS) and partial density of states (PDOS) of wz-ZnS and zb-ZnS using standard DFT and DFT + U methods which are shown in Fig. 1 and Fig. 2, respectively. The DOS features for both the phases are pretty similar, owing to the similarity in their structures. The DFT + U results for the optimum U_d^{opt} and U_p^{opt} pair offer a significant improvement over the standard DFT results. The positions of the peaks are now in excellent agreement with that obtained by Ley *et al.* [11] for zb-ZnS using x-ray spectroscopy as shown in Table III, which compares DOS features for DFT + U with the measured values, and other studies [51]. However, the application of the Hubbard terms does cause some undesirable deviations. The position of the S-3s levels has shifted towards the valence band maximum as compared to more accurate standard DFT results, which agreed well with the measured values. The width of the S-3s peak is also reduced for DFT + U calculation and is now significantly narrower than the measured values. Standard DFT did a good job at predicting the peak position and width of the S-3s levels. Moreover, the peak profile of the S-3p levels also matches well with the experimental results. The doublets in 3d peak are highly resolved for standard DFT but become more and more convoluted as U_d increases, which is in good agreement with the experimental results [11].

5. Effective mass

The transport properties and the photocatalytic activity of a material are dependent on the mobility of photogenerated electrons. For a smaller recombination rate of electron-hole pairs, faster movement of charge carriers is desired. The mobility of charge carriers is inversely proportional to their effective mass [52]

$$v = \frac{q\tau}{m^*} \tag{1}$$

where v is the mobility of carriers, τ is scattering time, q is the charge of carrier, and m^* is the effective mass. Effective mass is calculated using [53]

$$m^* = \hbar^2 \left(\frac{d^2E}{dk^2} \right)^{-1}, \tag{2}$$

where $\frac{d^2E}{dk^2}$ is the measure of the curvature of bands near the extrema, and $\hbar$ is the reduced Planck's constant. The curvature of bands in the vicinity of the Gamma point was obtained by performing a parabolic fit to the bands. Effective mass of electrons and holes are calculated using standard DFT (GGA) and GGA + U using our selected pair of U_p and U_d. The results for both the phases are summarized in Table IV. The results obtained using DFT + U are almost in agreement with some reported values [7,54]. As expected, the effective mass of holes is much greater than that of electrons. Due to high symmetry, for zb-ZnS, the electrons' effective masses along all directions (G → M, G → X, and G → R) calculated using DFT + U are similar. On the other hand, for wz ZnS, the electrons' effective masses are only similar along G → K and G → M directions. It's also evident that the effective mass of holes are more anisotropic than the electrons'.

6. Bulk modulus

The mechanical strength of the material is characterized by the elastic moduli. So the bulk modulus (B) and equilibrium lattice parameters for zb-ZnS and wz-ZnS are evaluated by fitting the total energies, calculated at different volumes for

TABLE III. Comparison of experimental and calculated DOS features. The labels (I_2, I_1, S_1, P_{II}, H_{IIB}, E_{II}, E_{III}, H_{IIIT}, P_{III}, H_{IIIB}, B) are from Ref. [11] for zb-ZnS.

Phase		I_2	I_1	S_1	P_{II}	H_{IIB}	E_{II}	E_{III}	H_{IIIT}	P_{III}	H_{IIIB}	B
Wurtzite	GGA	−1.32		−2.14	−4.57	−4.77	−4.92	−11.59	−11.75	−11.93	−12.25	−13.02
	DFT(GGA)+U	−1.42	−2.01	−2.58	−5.54	−5.93	−6.34	−11.11	−11.215	−11.33	−11.45	−11.54
Zinc blende	GGA	−1.3	−1.62	−2.75	−4.45	−4.64	−5.14	−11.58	−11.75	−11.93	−12.23	−13.08
	DFT(GGA)+U		−2.43	−2.79	−5.38	−5.81	−6.57	−11.07	−11.14	−11.27	−11.39	−11.48
	BZW-EF [51]	2	2.5		−4.5	−6.25				−12.3		
	Expt. [11]	−2	−2.6	−3.2	−4.9	−5.9	−6.4	−11.4	−11.8	−12.4	−13.3	−13.8

both the structures, with the Murnaghan's equation of state (M-EOS) [55],

$$E(V) = E(V_0) + \frac{BV}{B'}\left[\frac{(V_0/V)^{B'}}{B'-1} + 1\right] - \frac{BV_0}{B'-1} \quad (3)$$

where $E(V)$ is the energy at volume V, V_0 is the equilibrium volume, B is the bulk modulus, and B' is the first derivative of bulk modulus with respect to pressure. Figure 7 shows the variation of total energy with change in lattice volume for zb-ZnS and wz-ZnS. The equilibrium lattice constant for zb-ZnS, from M-EOS comes out to be 5.410 Å, which is very close to the value we got using BFGS algorithm and agrees well with the experimental 5.409 Å. The bulk modulus, for the zb phase, calculated using M-EOS, is 81.2 GPa and it is quite close to the measured value of ∼77 GPa [56,57]. The calculated value of derivative of bulk modulus (B') is 4.26, which also matches very well with the experimental value of 4.41 in Ref. [58] and 4.7 in Ref. [57]. Similarly for wz-ZnS the value of B and B' are 81.9 GPa and 3.96, respectively, which are in reasonable agreement with the experimental 76.9 GPa and 4.9 [58]. Gopal *et al.* have reported values similar to ours, i.e., 81 GPa and 80 GPa calculated by using SIRC and ACBN0, respectively, for both the zb phase and wz phase [32]. We have also calculated the bulk modulus without the Hubbard corrections (GGA) and gotten a value of 69 GPa for zb-ZnS and 69.6 GPa for wz phase which are severely underestimated. These results are similar to previously reported values in Ref. [32]. These findings once again verify that our proposed values of U_p and U_d for zb and wz-ZnS are successful to a great extent, in predicting the experimentally observed structural and electronic properties as compared to GW, HSE methods (see Table V).

B. Nanoclusters

In the last section we saw that the DFT + U framework is extremely successful in predicting most of the bulk properties very accurately. The accuracy is even better than the expensive hybrid HSE functionals in some departments. Now we implement the DFT + U framework to study small nanoclusters of Zn_nS_n. Since the two sets of Hubbard

TABLE IV. Effective mass of electrons and holes for zb-ZnS and wz-ZnS along specific directions in reciprocal space using standard DFT-GGA and DFT + U. The results are compared with reported values.

Phase		m_e^*/m_0			m_h^*/m_0		
	Direction	G → K	G → M	G → A	G → K	G → M	G → A
		(120)	(010)	(001)	(120)	(010)	(001)
	GGA	0.210	0.257	0.254	0.651	0.985	0.999
	DFT(GGA)+U	0.274	0.238	0.208	0.561	0.914	1.005
	LDA [7]	0.172	0.172	0.151	1.517	1.517	1.500
Wurtzite	PBE0 [54]	0.209	0.208	0.160	0.284	0.225	1.257
	GGA [54]	0.195	0.200	0.172	1.601	1.678	1.637
	GGA [7]	0.184	0.184	0.158	1.611	1.611	1.589
	LDA+U [7]	0.176	0.176	0.159	1.759	1.759	1.763
	Expt. [7]			0.280	0.490	0.490	1.400
	Direction	G → M	G → X	G → R	G → M	G → X	G → R
		(110)	(100)	(111)	(110)	(100)	(111)
	GGA	0.65	0.32	0.50	2.999	1.01	2.064
	DFT(GGA)+U	0.332	0.318	0.353	2.643	0.807	1.844
	LDA [7]	0.155	0.155	0.155	3.405	0.662	1.467
Zinc blende	PBE0 [54]	0.198	0.195	0.200	2.526	0.590	1.121
	GGA [54]	0.184	0.182	0.185	3.572	0.721	1.549
	GGA [7]	0.172	0.172	0.172	3.800	0.710	1.500
	LDA+U [7]	0.177	0.177	0.177	4.318	1.674	
	BZW-EF [51]	0.162	0.174	0.154	1.066	1.772	1.550
	Expt. [7]	0.340	0.340	0.340			1.760

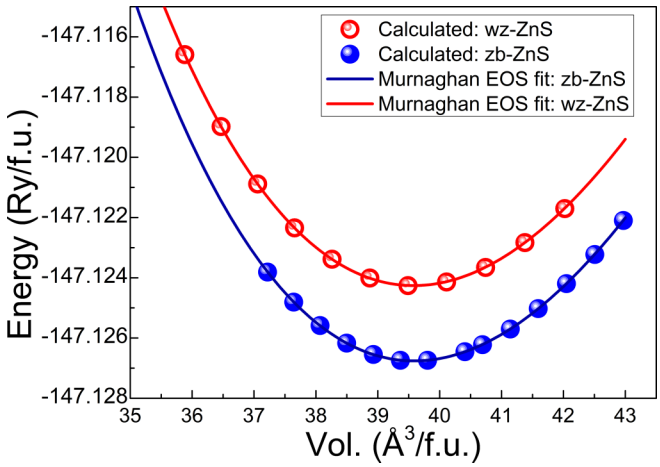

FIG. 7. Total energy vs volume per formula unit of ZnS for zb-ZnS and wz-ZnS. The symbols denote the calculated energies while the lines show the fitted Murnaghan equation of state.

corrections determined earlier for the two phases of ZnS are very similar, and there is no *a priori* reason to choose one over the other for the nanoclusters, we arbitrarily choose the parameters corresponding to wz-ZnS, i.e., $U_d = 10$ eV and $U_p = 5.049$ eV. The standard procedure in the study of nanoclusters is to conduct an unbiased search over the potential energy surface using genetic algorithms to find all the local minima of the nanoclusters of a particular size. The structure with the lowest energy gives the global minimum (GM). As previously mentioned, a lot of prior studies [25–27,33] on Zn_nS_n nanoclusters have provided the structures of local as well as global minima. Considering that we wish only to compare and examine the performance and reliability of DFT + U in predicting the properties of ZnS nanoclusters, we decided not to conduct such a time consuming search over the entire potential energy landscape and rather relied on the results from the previous studies to get an initial geometry for the global as well as local minima. Structural properties such as the bond lengths and bond angles were analyzed. We also calculate the HOMO-LUMO gap (E_g) and the cohesive energies ($E_{\rm coh}$). Cohesive energy was used as a measure of the stability of nanoclusters for a fixed n to rank them by their stability. The formula used was:

$$E_{\rm coh} = -E(\mathrm{Zn_nS_n})/n + E(\mathrm{Zn}) + E(\mathrm{S}) \qquad (4)$$

where $E(Zn)$ and $E(S)$ is the energy of isolated Zn and S atom respectively, $E_{\rm coh}$ is the cohesive energy, and $E(\mathrm{Zn_nS_n})$ is the energy of the nanocluster with n formula units of ZnS.

Table VI summarizes the various structural as well as the electronic properties obtained using our DFT + U calculations as well as previous calculations using B3LYP [25–27] and GGA [33] functionals. Figure 8 shows the optimized structures of global minimum for different n. Figure 9 shows the optimized structures of top ranking local minima for different n. The Cartesian coordinates of structures of global as well as local minima are provided in the Supplemental Material [60].

By analyzing the cohesive energies of all the stable structures for each n we found that, similar to previous studies, ringlike structures are the most stable for $n = 2 - 5$ while 3d

TABLE V. Comparison of lattice parameters, band gaps (E_g), average d-band energies (E_d), bulk modulus (B), and it's derivative (B') calculated using various computational methods. Experimental values are from Refs. [6,7,11,15,39,40,47,56,57].

Method	Phase	a (Å)	c (Å)	E_g (eV)	E_d (eV)	B (GPa)	B'
GGA-PBE	wz	3.849	6.309	2.06	−5.95	69.6	4.37
	zb	5.447		2.01	−5.89	69	4.76
DFT(GGA)+U	wz	3.821	6.25	3.873	−9.358	81.9	3.96
	zb	5.408		3.701	−9.274	81.2	4.26
LDA [7]	wz			1.99	−6.5		
	zb			1.875	−6.1		
LDA+U [7]	wz			2.283	−8.2		
	zb			2.332	−9		
GW [59]	wz						
	zb			3.54	−6.95		
PBE0 [54]	wz	3.843	6.299	3.69			
	zb	5.44		3.2			
HSE [32]	wz	3.85	6.271	3.42	−7.5	74	
	zb	5.432		3.49	−7.5	74.4	
GGA-PBE [32]	wz	3.88	6.3	2.1	−6	60	
	zb	5.489		2.23	−6	68	
SIRC [32]	wz	3.83	6.28	3.6		81	
	zb	5.421		3.6		81	
ACBN0 [32]	wz	3.851	6.278	3.31	−11.7	79	
	zb	5.437		3.42	−11.7	80	
BZW-EF [51]	wz						
	zb	5.409		3.725		78	
Expt.	wz	3.822	6.26	3.86	−9	76.9	4.9
	zb	5.409		3.7	−9	77	4.41

TABLE VI. Structural properties, HOMO-LUMO gap (E_g), and cohesive energies (E_{coh}) of Zn_nS_n nanoclusters.

i	Method	Symmetry	Zn-S (Å)	S-Zn-S (deg)	Zn-S-Zn (deg)	E_{coh} (eV)	E_g (eV)
2	DFT + U	D_{2h}	2.2	112.7	67.3	3.988	3.100
	B3LYP/6-311+G* [26]	D_{2h}				5.1	2.78
	B3LYP/SKBJ(d) [25]	D_{2h}	2.27	114.5		2.963	
	GGA[33]	D_{2h}	2.24			4.66	
3	DFT + U	D_{3h}	2.14	153.8–153.9	86.1–86.3	5.037	4.553
	B3LYP/6-311+G* [26]	D_{3h}				5.89	4.19
	B3LYP/SKBJ(d) [25]	D_{3h}	2.21	157.8		3.888	
	GGA [33]	D_{3h}	2.17	160	80.2	5.67	
4	DFT+U	D_{4h}	2.12	171.8	98.2	5.276	4.758
	B3LYP/6-311+G* [26]	D_{4h}		180	93.4	4.85	4.49
	B3LYP/SKBJ(d) [25]	D_{4h}	2.19	177.4		4.07	
	GGA [33]	D_{4h}	2.15	180	91	5.87	3
5	DFT + U	C_s	1.76	167.9–168	120–120.1	5.324	5.073
	B3LYP/6-311+G* [26]	C_s				4.39	4.59
	B3LYP/SKBJ(d) [25]	C_s	2.18	178.9		4.092	
	GGA [33]	C_{1h}	2.15	176	94.5	5.91	3.32
6	DFT + U	D_{3d}	2.25–2.41	172.6–172.8	127.2–127.5	5.427	3.933
	B3LYP/6-311+G* [26]	D_{3d}				4.91	3.88
	B3LYP/SKBJ(d) [25]	D_{3d}	2.31–2.47	140.55		4.178	
	GGA [33]	D_{3d}	2.27			6.04	2.54
7	DFT + U	C_1	2.09–2.44	94.8–159.2	71.7–111.2	5.433	3.980
	B3LYP/6-311+G* [26]	C_{3v}	2.29–2.37			4.41	3.82
	B3LYP/SKBJ(d) [25]	C_{2v}	2.20–2.58	97.4–175.0		4.251	
	GGA [33]	C_{2v}	2.23			6.03	2.13
8	DFT + U	S_4	2.22–2.37	99.7–134.1	74.3–108.9	5.609	4.131
	B3LYP/6-311+G* [26]	S_4				5.55	4.06
	B3LYP/SKBJ(d) [25]	S_4	2.28–2.42	100.3–137.1		4.323	
	GGA [33]	S_4	2.21			6.19	2.75
9	DFT + U	C_{3h}	2.22–2.33	99.8–134.6	76.5–107.2	5.691	4.203
	B3LYP/6-311+G* [26]	C_{3h}				5.12	4.16
	B3LYP/SKBJ(d) [25]	C_{3h}	2.28–2.33	103.8–138.0		4.388	
	GGA [33]	C_{3h}	2.32			6.26	2.81
10	DFT + U	C_1	2.1–2.37	96.6–161.7	75.8–111.7	5.692	3.996
	B3LYP/6-311+G* [26]	C_3				4.64	4.04
	B3LYP/SKBJ(d) [25]						
	GGA [33]						
11	DFT + U	C_s	2.21–2.34	95.0–129.4	75.6–109.6	5.787	4.200
	B3LYP/6-311+G* [26]	C_s				5.36	4.17
	B3LYP/SKBJ(d) [25]						
	GGA [33]						

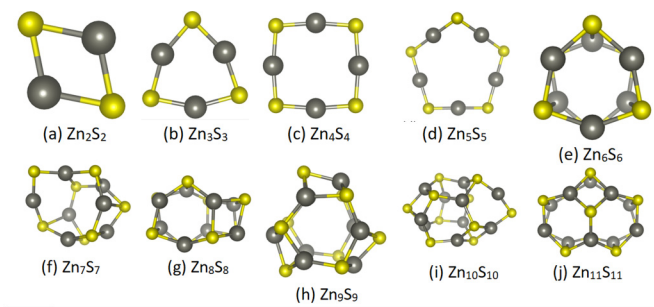

FIG. 8. Global minima structures of Zn_nS_n nanoclusters for $n = 2 - 11$. The gray colored atoms are Zn and the yellow colored atoms are S.

structures are the most stable for $n > 5$. The GM for Zn_2S_2 is a planar ring [Fig. 8(a), D_{2h}] with alternate Zn and S atoms. The Zn-S bond length is 2.20 Å, S-Zn-S bond angle is 112.7°, and Zn-S-Zn bond angle is 67.3°. This structure is 0.873 eV more stable than the next lowest energy structure [Fig. 9(a), C_{2v}] with consecutive Zn and S atoms. For $n = 3$ we studied various 2d structures (Fig. 9) and found that the global minimum structure is a hexagon [Fig. 8(b), D_{3h}] with Zn-S bond length=2.14 Å, S-Zn-S bond angle =153.8°, and Zn-S-Zn bond angle=86.1°. Zn_4S_4 is observed to have a squarelike structure [Fig. 8(c), D_{4h}]. While previous studies indicate the S-ZnS bond angle to be almost 180°, we found that the bonds weren't exactly linear. A 3d boxlike Euler structure [Fig. 9(d), T_d] is found to be 0.342 eV above the

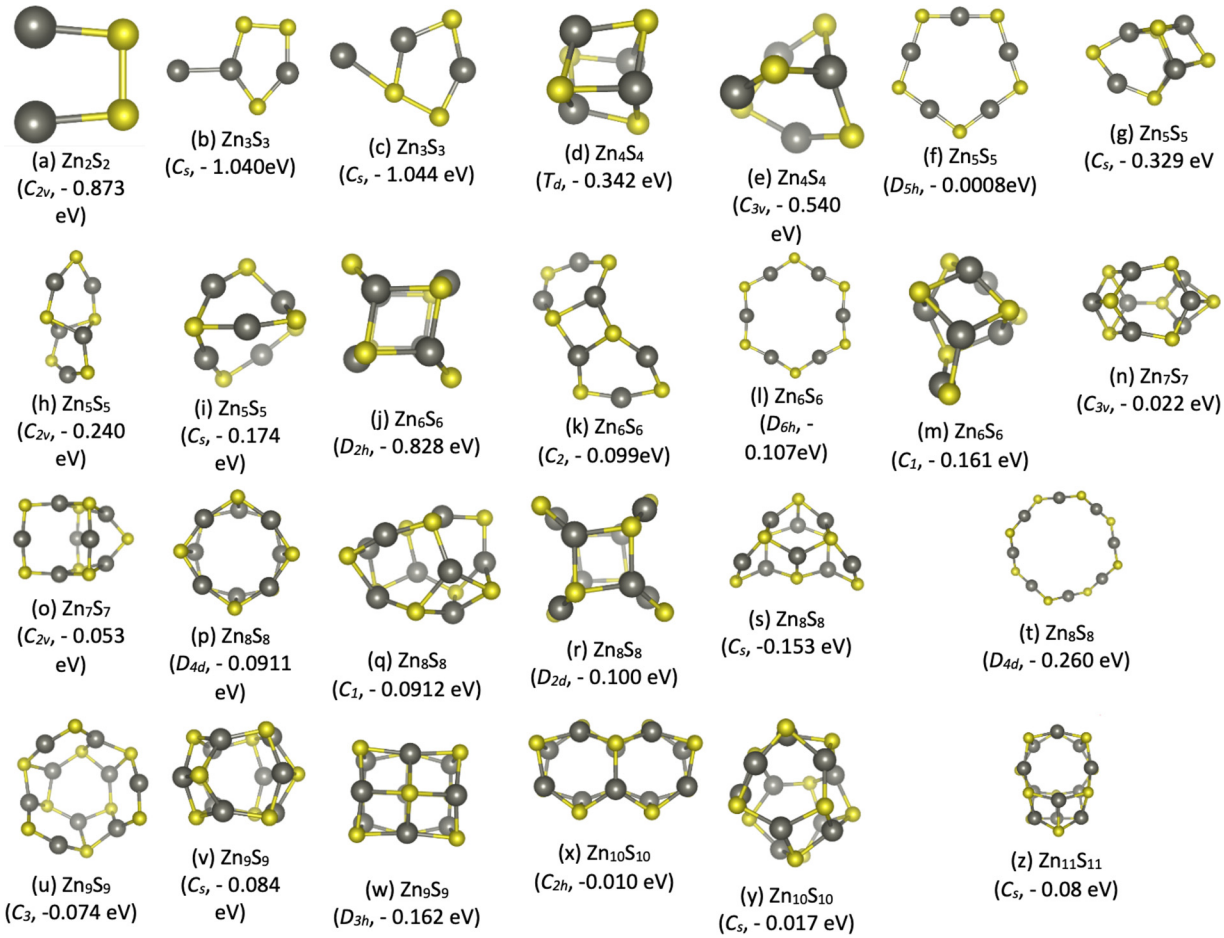

FIG. 9. Structures of local minima for $n = 2 - 11$ as well as the point groups and the difference in cohesive energies as compared to the global minimum. The gray colored atoms are Zn and the yellow colored atoms are S.

GM. Similar to previous studies, a bent-ring- (pentagon-) [Fig. 8(d), C_s] like structure is found to be the most stable one for Zn_5S_5. The 3d structures [Figs. 9(f)–9(i)] are found to have higher energies. $n = 5$ also marks the transition point beyond which 3d structures are more stable. For $n = 6$ a drumlike structure, [Fig. 8(e), D_{3d}] made up of two parallel (hexagonal) rings, joined together by Zn_2S_2 rings is found to be the GM. The lowest energy structure for Zn_7S_7 is found to be different from any other prior study. The global minimum structure [Fig. 8(f), C_1] is made up of a Zn_3S_3 ring and a bent Zn_4S_4 ring linked together by Zn_2S_2 rings. In fact, we found the second lowest energy structure [Fig. 9(n), C_{3v}] of Zn_7S_7 with $\Delta E_{\text{coh}} = -0.022$ eV to be similar to the GM reported by Burnin *et al.* [26], whereas the basketlike structure [Fig. 9(o), C_{2v}] reported as GM in Refs. [25,33] was found to be third lowest in energy with $\Delta E_{\text{coh}} = -0.053$ eV. We also note here that the GM reported in Ref. [27], looks very similar to ours. For $n = 8$, a 3d structure [Fig. 8(g), S_4] that consists of Zn_2S_2 and Zn_3S_3 rings is found to be the most stable, while the ringlike structure is the least stable. The most stable structure of Zn_9S_9 consists of Zn_3S_3 and Zn_2S_2 rings. A tubelike structure [Fig. 9(w)] was found to be the least stable. For $n = 10$ the lowest energy structure [Fig. 8(i), C_1] is in disagreement with previous calculations. Moreover, none of the prior studies have even reported a similar structure as being the local minimum. The peculiar structure consists of four Zn_3S_3 rings, five Zn_2S_2 rings, and one Zn_4S_4 ring. The structure reported by Hamad *et al.* was found to be a local minimum [Fig. 9(x)] in our study, while the one reported by Burnin *et al.* wasn't found at all. The structure of $Zn_{11}S_{11}$ [Fig. 8(j), C_s] was found to be similar to previously determined structures [26,28].

Overall, in stark contrast to the previous studies, done using the B3LYP functional, we found that the bond angles were slightly smaller in comparison using DFT + U. The HOMO-LUMO gaps (E_g), although overestimated as compared to B3LYP, show remarkable improvement over those obtained through GGA [33]. The values match very closely to those obtained by Burnin *et al.* [27], and AlSunaidi [27] using B3LYP functionals. However, we should note here that for $n = 7$ and $n = 10$, this comparison is meaningless due to the different GMs obtained in our study. The gaps (E_g) didn't seem to follow any particular trend and showed random ups and downs. The gaps were always larger than the bulk band gap except for $n = 2$. Therefore, determination of HOMO-LUMO gaps is one area where DFT + U seems to do very well at very cheap computational cost. In order to confirm that the unique GM obtained for $n = 7$ and $n = 10$ weren't an artifact of the Hubbard correction, we also performed a B3LYP-TZVP study for the controversial

structures [Fig. 8(f), Figs. 9(n) and 9(o)]. The results corroborate our DFT + U results, with the energies of the structures coming out to be in the exact same sequence. Moreover, the cohesive energy differences with GM were also very similar.

IV. CONCLUSION

The present work discussed the optimization of Hubbard corrections (U_p and U_d) empirically using the band-gap and d-band positions of the bulk ZnS as benchmarks. Using these, DFT + U study was performed for bulk ZnS and ZnS nanoclusters. The bulk structural and electronic properties were determined to be in excellent agreement with experimentally measured values. The accuracy was found to be similar or better than higher levels of theory (hybrid functionals, GW approximation) which are extremely computationally expensive. The structural and electronic properties of energetically most favorable nanoclusters were in reasonable agreement with previous studies performed using expensive B3LYP hybrid functionals. The HOMO-LUMO gaps were very close to that predicted by more accurate and expensive functionals. For $n = 7$ and $n = 10$ previously unknown global minima were found, while several previously unreported local minima structures were studied for different n. Various important extrinsic material properties including the effect of metal doping (e.g., Cu and Al) on band-gap tunability of ZnS, spin resolved transport in p-type ZnS etc. can be calculated more accurately. This will facilitate the designing of devices for applications in dye-sensitized solar cells and biosensors.

ACKNOWLEDGMENTS

We acknowledge the High Performance Computing Facility at the Inter University Accelerator Centre (IUAC), New Delhi for providing valuable computational resources. D.M. acknowledges the financial support from UGC through Grant No. F.4-5(202-FRP)/2015(BSR). M.S. thanks P. Bhasin for valuable discussions.

[1] P. Sebastian and M. Ocampo, Sol. Energy Mater. Sol. Cells **44**, 1 (1996).
[2] D. Halliday, J. Eggleston, and K. Durose, Thin Solid Films **322**, 314 (1998).
[3] Y. Jiang, W. Zhang, J. Jie, X. Meng, J. Zapien, and S.-T. Lee, Adv. Mater. **18**, 1527 (2006).
[4] S. Farhangfar, R. B. Yang, M. Pelletier, and K. Nielsch, Nanotechnology **20**, 325602 (2009).
[5] P. Jiang, J. Jie, Y. Yu, Z. Wang, C. Xie, X. Zhang, C. Wu, L. Wang, Z. Zhu, and L. Luo, J. Mater. Chem. **22**, 6856 (2012).
[6] S. Ves, U. Schwarz, N. E. Christensen, K. Syassen, and M. Cardona, Phys. Rev. B **42**, 9113 (1990).
[7] S. Z. Karazhanov, P. Ravindran, A. Kjekshus, H. Fjellvg, U. Grossner, and B. G. Svensson, J. Appl. Phys. **100**, 043709 (2006).
[8] J. P. Perdew and A. Zunger, Phys. Rev. B **23**, 5048 (1981).
[9] J. P. Perdew, K. Burke, and M. Ernzerhof, Phys. Rev. Lett. **77**, 3865 (1996).
[10] D. Vogel, P. Krüger, and J. Pollmann, Phys. Rev. B **54**, 5495 (1996).
[11] L. Ley, R. A. Pollak, F. R. McFeely, S. P. Kowalczyk, and D. A. Shirley, Phys. Rev. B **9**, 600 (1974).
[12] J. P. Perdew and M. Levy, Phys. Rev. Lett. **51**, 1884 (1983).
[13] L. J. Sham and M. Schlüter, Phys. Rev. Lett. **51**, 1888 (1983).
[14] J. P. Perdew, R. G. Parr, M. Levy, and J. L. Balduz, Phys. Rev. Lett. **49**, 1691 (1982).
[15] D. Vogel, P. Krüger, and J. Pollmann, Phys. Rev. B **52**, R14316(R) (1995).
[16] F. Aryasetiawanand and O. Gunnarsson, Rep. Prog. Phys. **61**, 237 (1998).
[17] A. I. Liechtenstein, V. I. Anisimov, and J. Zaanen, Phys. Rev. B **52**, R5467 (1995).
[18] V. I. Anisimov, F. Aryasetiawan, and A. I. Lichtenstein, J. Phys.: Condens. Matter **9**, 767 (1997).
[19] J. Heyd, G. E. Scuseria, and M. Ernzerhof, J. Chem. Phys. **118**, 8207 (2003).
[20] J. Heyd, G. E. Scuseria, and M. Ernzerhof, J. Chem. Phys. **124**, 219906 (2006).
[21] E. Şaşioğlu, C. Friedrich, and S. Blügel, Phys. Rev. B **83**, 121101(R) (2011).
[22] M. Cococcioni and S. de Gironcoli, Phys. Rev. B **71**, 035105 (2005).
[23] O. Gunnarsson, O. K. Andersen, O. Jepsen, and J. Zaanen, Phys. Rev. B **39**, 1708 (1989).
[24] M. Springer and F. Aryasetiawan, Phys. Rev. B **57**, 4364 (1998).
[25] J. M. Matxain, J. E. Fowler, and J. M. Ugalde, Phys. Rev. A **61**, 053201 (2000).
[26] A. Burnin, E. Sanville, and J. J. BelBruno, J. Phys. Chem. A **109**, 5026 (2005).
[27] A. AlSunaidi, AIP Conf. Proc. **929**, 43 (2007).
[28] S. Hamad, C. R. A. Catlow, E. Span, J. M. Matxain, and J. M. Ugalde, J. Phys. Chem. B **109**, 2703 (2005).
[29] A. D. Becke, J. Chem. Phys. **98**, 5648 (1993).
[30] C. Lee, W. Yang, and R. G. Parr, Phys. Rev. B **37**, 785 (1988).
[31] P. Giannozzi, S. Baroni, N. Bonini, M. Calandra, R. Car, C. Cavazzoni, D. Ceresoli, G. L. Chiarotti, M. Cococcioni, and I. e. a. Dabo, J. Phys.: Condens. Matter **21**, 395502 (2009).
[32] P. Gopal, M. Fornari, S. Curtarolo, L. A. Agapito, L. S. I. Liyanage, and M. B. Nardelli, Phys. Rev. B **91**, 245202 (2015).
[33] D. L. Lalsareand and A. Kshirsagar, Bull. Mater. Sci. **35**, 1055 (2012).
[34] K. Momma and F. Izumi, J. Appl. Crystallogr. **44**, 1272 (2011).
[35] BURAI 1.3: A GUI of QUANTUM ESPRESSO code, https://github.com/BURAI-team/burai.
[36] Jmol: an open-source Java viewer for chemical structures in 3D, http://www.jmol.org/.
[37] D. Vanderbilt, Phys. Rev. B **41**, 7892 (1990).
[38] H. J. Monkhorst and J. D. Pack, Phys. Rev. B **13**, 5188 (1976).
[39] E. H. Kisi and M. M. Elcombe, Acta Crystallogr. Sect. C **45**, 1867 (1989).
[40] M. Kh. Rabadanov, Kristallografiya **40**, 21 (1995).
[41] C. G. Broyden, IMA J. Appl. Math. **6**, 222 (1970).

[42] R. Fletcher, Comput. J. **13**, 317 (1970).
[43] D. Goldfarb, Math. Comput. **24**, 23 (1970).
[44] D. F. Shanno, Math. Comput. **24**, 647 (1970).
[45] F. Weigendand and R. Ahlrichs, Phys. Chem. Chem. Phys. **7**, 3297 (2005).
[46] F. Neese, Wiley Interdisc. Rev.: Comput. Molec. Sci. **2**, 73 (2011).
[47] R. Weidemann, H.-E. Gumlich, M. Kupsch, H.-U. Middelmann, and U. Becker, Phys. Rev. B **45**, 1172 (1992).
[48] P.-O. Löwdin, Adv. Quantum Chem. **5**, 185 (1970).
[49] L. A. Agapito, S. Curtarolo, and M. Buongiorno Nardelli, Phys. Rev. X **5**, 011006 (2015).
[50] E. Goh, J. Mah, and T. Yoon, Comput. Mater. Sci. **138**, 111 (2017).
[51] B. Khamala, L. Franklin, Y. Malozovsky, A. Stewart, H. Saleem, and D. Bagayoko, Comput. Condens. Matter **6**, 18 (2016).
[52] M. Nolan and S. D. Elliott, Phys. Chem. Chem. Phys. **8**, 5350 (2006).
[53] J. Zhang, P. Zhou, J. Liu, and J. Yu, Phys. Chem. Chem. Phys. **16**, 20382 (2014).
[54] M. Dong, J. Zhang, and J. Yu, APL Mater. **3**, 104404 (2015).
[55] F. D. Murnaghan, Proc. Natl. Acad. Sci. USA **30**, 244 (1944).
[56] M. L. Cohen, Phys. Rev. B **32**, 7988 (1985).
[57] P. K. Lam, M. L. Cohen, and G. Martinez, Phys. Rev. B **35**, 9190 (1987).
[58] M. Bilge, S. Özdemir Kart, H. H. Kart, and T. Cagin, J. Achiev. Mater. Manufac. Eng. **31**, 29 (2008).
[59] T. Miyake, P. Zhang, M. L. Cohen, and S. G. Louie, Phys. Rev. B **74**, 245213 (2006).
[60] See Supplemental Material at http://link.aps.org/supplemental/10.1103/PhysRevB.100.045151 for Cartesian coordinates of local and global minima of nanoclusters.